Mon. Not. R. Astron. Soc. **274,** 523–543 (1995)

Collisional redistribution effects on line polarization in spherical atmospheres

K. N. Nagendra
Indian Institute of Astrophysics, Bangalore 560034, India

Accepted 1994 December 16. Received 1994 December 14; in original form 1994 September 9

ABSTRACT

The polarization of resonance and subordinate lines formed in spherically symmetric media is studied. The effect of collisions is shown by taking a combination of partial redistribution mechanisms represented by the functions $R_{\mathrm{II-A}}(x, x')$ and $R_{\mathrm{III-A}}(x, x')$, which are well-known redistribution functions that describe interaction of line photons with a two-level model atom. A large number of models are presented, which clearly show the effect of collisions on line polarization, when basic model parameters of a two-level atom are varied one at a time. Thus the grid of models generated serves to establish upper and lower limits on the impact of collisions on line polarization. Some results employing a more accurate treatment of collisional redistribution are also shown. The purpose of this paper is to understand the quantitative behaviour of line polarization when collisional redistribution plays an important role in the transfer of line radiation.

Key words: atomic processes – line: formation – polarization – radiative transfer – scattering.

1 INTRODUCTION

The polarization of an emergent spectral line is caused by the anisotropy of the medium in which the line is formed. In this paper, we are basically concerned with the non-magnetic anisotropy caused by virtue of atomic level configuration of the transition involved. This is generally referred to as polarization by resonance scattering of radiation on atoms. Hence there is no polarization in the absence of scattering in the medium. The resonance scattering in resonance lines (for which the lower level of the transition is not broadened) is a well-explored subject (see Rees 1987, Rees & Murphy 1987 and Ivanov 1991 for the historical development and the unsolved problems in this area). In a series of papers, Faurobert-Scholl (1987, 1988, 1991, 1992, 1993) has studied various aspects of this interesting topic. In an important paper, Rees & Saliba (1982) explored the salient features of the partial redistribution effects in resonance scattering in resonance lines. These authors made a suggestion that the intricate angle and frequency coupling that exists in the 'angle-dependent frequency redistribution matrix' can be decoupled by expressing it as product of a frequency redistribution scalar function and an angle-dependent polarization phase matrix. This so-called hybrid model has since been practically most useful in solving this numerically difficult problem of line formation with angle-dependent polarization redistribution matrices (see Faurobert-Scholl 1987 for a comparison of angle-dependent and angle-averaged solutions employing this hybrid model). The resonance line polarization problem in spherically symmetric media is solved by Nagendra (1986, 1988). The angle–frequency coupling of polarized radiation field is strong in outermost shallow layers of a spherical atmosphere, particularly in extended spherical atmospheres, due to natural peaking of the radiation field as the ray travels outwards in optically thin layers. This peaking of radiation, called the curvature effect, makes the radiative transfer computation in spherical geometry even more expensive due to severe numerical demands on spatial and angular resolution of diffuse radiation field prevailing in these outer layers. In our earlier papers (Nagendra 1988, 1989), the role played by collisions is neglected *ab initio.* Saliba (1985) presented the first computation of resonance line formation in planar media when collisional redistribution is included through a combination of functions $R_{\mathrm{II-A}}(x, x')$ and $R_{\mathrm{III-A}}(x, x')$. He employed a realistic solar atmosphere and depth-dependent branching ratios to model theoretically the observed solar resonance line polarization. Recently, Faurobert-Scholl (1992, 1993) has employed a more involved collisional redistribution matrix developed by Domke & Hubeny (1988) to model the

observations of solar resonance line polarization. It is shown that the collisional redistribution has a significant influence on the polarization of resonance lines. Heinzel & Hubeny (1982) suggested a method of including collisional effects in subordinate lines, through a combination of redistribution functions $R_{\mathrm{V-A}}(x, x')$ and $R_{\mathrm{III-A}}(x, x')$, without including the polarization of radiation. The corresponding combination for resonance lines is very well known. All the references mentioned above, except Nagendra (1988), employ plane-parallel (PP) stratification. In this paper, we have studied the effect of collisions on both resonance and subordinate lines formed in spherically symmetric (SS) media. Simple parametrized models of collisional redistribution are employed for this purpose. We describe our computations in Section 2. The relevant equations, method of computation, and model parametrization are presented in Nagendra (1988) for polarized line transfer in SS media. Hence we do not repeat them here. The collisional redistribution functions for both resonance and subordinate lines are studied in Hubeny & Heinzel (1984), the results of which, as well as the results presented in Nagendra (1994), supplement the discussion in Section 2 on collisional redistribution. Specific conclusions are drawn at the end of each of Sections 2.1–2.10. The general conclusions are presented in Section 3.

2 RESULTS AND DISCUSSION

In this section, we present the results of our computations using parametrized models. One of the essential parameters of the two-level atom model is ϵ, the probability that a photon is destroyed by collisional de-excitation during scattering – also called the thermalization parameter. The range of variation of this probability factor is [0, 1]. The case $\epsilon = 1$ refers to the pure-LTE case. Other values of ϵ refer to the non-LTE (NLTE) situation. The extreme case of $\epsilon = 0$ means that the atmosphere is a purely scattering medium. As ϵ increases, starting from zero, the thermalization of photons also increases. In other words, the thermal coupling with continuum radiation field increases due to an increase in the number of collisions instead of scatterings. We have assumed the overlapping continuum to be purely absorbing. The continuum radiation is unpolarized (since there is no continuum scattering). Hence the stronger the coupling is with the continuum, the weaker are the anisotropy and polarization of line radiation. The variation of ϵ forms a sequence of models shown in Fig. 1. The parameter β^{C} is the ratio of continuum opacity to frequency-averaged line opacity, $\beta^{\mathrm{C}} = k^{\mathrm{C}}(r)/k^{\mathrm{L}}(r)$. In all the models presented in this paper, we have taken an inverse-square variation of both these opacities. Hence β^{C} is a constant throughout the spherical shell atmosphere. The variation of β^{C}, however, forms another sequence of models, shown in Fig. 2. The parameter T^{L} is the frequency-averaged line centre optical depth. The variation of T^{L} forms the sequence of models shown in Fig. 3. Another important free parameter of the models is the damping parameter $a = \Gamma/4\pi\Delta\nu_{\mathrm{D}}$, where Γ is the sum of radiative and collisional broadening rates. The factor $\Delta\nu_{\mathrm{D}}$ is a constant Doppler width, for the isothermal models presented here. The variation of a forms a sequence of models shown in Fig. 4. The dimensionless outer radius of the spherical shell ($r = R$) is also an important free parameter (note that the inner boundary of the spherical shell is at a non-dimensional radius $r = 1$ measured in the units of core radius r_{core}). The larger the value of R is, the more extended is the atmosphere. We have presented a sequence of models in Fig. 6, showing the effect of variation of R on the emergent polarization profiles. Depending on the evolutionary and dynamical state of the stellar atmosphere, the density distribution in a spherical atmosphere may generally have a power-law-type opacity distribution $k^{\mathrm{L}}(r) = Kr^{-n}$ ($n = -3$, -2, -1, 0, 1, 2, 3 etc.) or can be expressed as a combination thereof. We have computed a sequence of models, shown in Fig. 7, by varying the opacity power-law index n. In the same manner as opacity, the local Planck function can also vary in the form of a power law, depending on the temperature structure in the region of line formation. We have computed a sequence of models, shown in Fig. 8, in which the radial variation of Planck function in a form $B(r) = B_0 r^{-m}$ ($m = -2$, -1, 0, 1, 2) is considered. We have also shown a set of models in which the exact Domke–Hubeny (DH) collisional redistribution matrix is employed instead of the schematic approach involving the branching ratio between $R_{\mathrm{II-A}}(x, x')$ and $R_{\mathrm{III-A}}(x, x')$. The results are shown in Fig. 9. The electron scattering contribution is parametrized through $\beta^{\mathrm{e}} = k^{\mathrm{e}}(r)/k^{\mathrm{L}}(r)$, defined in the same way as the continuum absorption parameter β^{C}. The variation of β^{e} forms the sequence of models shown in Fig. 10. The non-coherence fraction Λ is the branching ratio between purely coherent and purely non-coherent scattering in the atoms' frame. Correspondingly, it is a branching ratio between $R_{\mathrm{II-A}}(x, x')$ and $R_{\mathrm{III-A}}(x, x')$ in the laboratory frame. The variation of this important parameter constitutes the sequence of models shown in Fig. 5. In all the figures the abscissa refers to the displacement from line centre in reduced frequency units $x = (\nu - \nu_0)/\Delta\nu_{\mathrm{D}}$. The ordinates refer to $\log I(x, \mu_1 = 0.11, \tau = 0)$ and the percentage of emergent polarization $p(x, \mu_1 = 0.11, \tau = 0)$. The variations of frequency-averaged source functions $S_I(\tau)$ and $S_Q(\tau)$ as a function of optical depth τ are also shown. Associated with each figure is a table listing some of the relevant escape probability quantities, which help in understanding the physical behaviour of models more quantitatively than just the emergent profiles. The basic two-level atom 'standard model parameters' remain the same for all the models, unless otherwise indicated inside the figure panel or in the figure caption and the corresponding table. This 'standard model' is represented by the following parameters: $\epsilon = 10^{-4}$; $\beta^{\mathrm{C}} = 10^{-4}$; $\beta^{\mathrm{e}} = 0$; $a_{\mathrm{u}} = 0.9 \times 10^{-2}$; $a_{\mathrm{l}} = 0.1 \times 10^{-2}$; $a = a_{\mathrm{u}} + a_{\mathrm{l}} = 10^{-2}$; $B(r) = 1$; $k^{\mathrm{L,C,e}}(r) = Kr^{-2}$; $T^{\mathrm{L}} = 10^6$; $\Lambda = 2/3$; $R = 3$. We employ the boundary conditions that no radiation is incident on the outer boundary of the spherical shell atmosphere, while the inner boundary is illuminated isotropically by an emitting opaque core at the centre. We stress again that the atmospheric and atomic models, boundary conditions etc. are exactly the same as in Nagendra (1988). Hence we do not need to repeat all the equations here. The equations necessary for dealing with DH generalized redistribution matrix are given in Nagendra (1994), and the same equations are used here also. These equations can also be found in Domke & Hubeny (1988) or Faurobert-Scholl (1992, 1993). We feel that no confusion is caused in this regard, since uniform and conventional notations and model parametrizations are employed in all our papers.

2.1 The effect of thermalization parameter ϵ

The results of computations are shown in Fig. 1. Some useful probabilistic quantities derived from the scaling laws are shown in Table 1 to aid the discussion of results. The values of ϵ are selected in such a way that the models 1–6 represent effectively very thin ($T_{\rm eff}=\epsilon T^{\rm L}=10^{-2}$) to effectively very thick ($T_{\rm eff}=10^{6}$) lines. The numbers shown near the curves give the model number. We identify the resonance line profiles by thin lines, and the corresponding cases of subordinate line profiles by heavy lines. As the value of ϵ increases, the magnitude of polarization generally decreases due to a decrease in the number of scatterings. Also, there is a gradual shift of positive polarization peak towards the line centre as the ϵ value is increased. Correspondingly, the intensity profiles become shallow (unsaturated) as $\epsilon\rightarrow 1$. Since the sphericity of the medium does not qualitatively affect the frequency dependence of I and p profiles, we employ the plane-parallel escape probability quantities (see Table 1) to interpret the results. Another general feature peculiar to SS media is that the LTE intensity profile is in emission, unlike the corresponding PP case. This is purely because of the geometrical effect, i.e., the larger emitting area contributing to line-core emission (which originates in outermost layers), compared to the area contributing to line-wing emission (which originates in inner layers). The importance of partial redistribution (PRD) effects in the line wings in the presence of continuum absorption is given by the condition $q\ll 1$ (Hubeny 1985a), where $q=(\pi^2\beta^{\rm C}/a)$. Since this condition is satisfied for all the models shown in Fig. 1, they are influenced by PRD effects – in other words, by the details of redistribution mechanism. However, the influence of continuum absorption in our models is responsible for most of the radiative transfer effect shown in this paper. It is shown by Frisch (1980, 1988) that line transfer problems employing $R_{\rm I}$, $R_{\rm III}$ and $R_{\rm V}$ have non-diffusive complete redistribution (CRD)-type asymptotic behaviour, whereas $R_{\rm II}$ has a diffusive type asymptotic behaviour both in frequency and space. This diffusive behaviour of $R_{\rm II}$ arises due to coherent trapping of line photons in the far wings during the scattering process. The deviation of the $R_{\rm V}$ source function from that of CRD is proportional to $a_{\rm u}/a_{\rm l}$, and hence increases as $a_{\rm l}\rightarrow 0$. For $R_{\rm V}$ redistribution, at each scattering, a photon absorbed in the wing has a probability $a_{\rm u}/(a_{\rm u}+a_{\rm l})$ of being re-emitted at the same frequency, and a probability $a_{\rm l}/(a_{\rm u}+a_{\rm l})$ of being re-emitted in the core. In our case, these probabilities are respectively 0.9 and 0.1.

The intensity source function $S_I(\tau)$ and the polarized source function $S_Q(\tau)$ define together the overall anisotropy existing at different optical depths in the spherical shell atmosphere. Since there is a correspondence between $S_I(\tau)$ and $I(x,\mu)$ and $S_Q(\tau)$ and $p(x,\mu)$, it is sometimes advantageous to plot $S_I(\tau)$ and $S_Q(\tau)$ together, to understand the behaviour of emergent quantities. The ϵ parameter affects the line formation physically through inelastic collisional deexcitation of atoms. On the other hand, $\beta^{\rm C}$ affects spectral lines through absorption and emission of line radiation in the overlapping continuum. To estimate which of these two processes is stronger, we compare the quantities $\tau_{\beta^{\rm C}}(x_{\beta^{\rm C}})$ and $\tau_\epsilon(x_\epsilon)$, which are respectively the characteristic depths at the corresponding characteristic frequencies $x_{\beta^{\rm C}}$ and x_ϵ. As shown by Hubeny (1985a), the process which is responsible for 'frequency thermalization' (FT) of the source function is the one that dominates the transfer in the line profile. The FT mechanism refers to the frequency diffusion process leading to the arrival of PRD line-wing photons at the core ($x<3$), where subsequent line scatterings can be described by the CRD function itself, before the photon finally escapes from the medium. Since our models are effectively thick (except for model 1), and even optically thick [$T_{\rm opt}=(aT^{\rm L})^{1/3}>1$)], the FT is very effective in the coupling of core and wing frequency regions of the line profile. According to Hubeny (1985a), we have

$$\tau_{\rm FT}=\min[\tau_\epsilon(x_\epsilon),\,\tau_{\beta^{\rm C}}(x_{\beta^{\rm C}})], \tag{1a}$$

where

$$\tau_\epsilon(x_\epsilon)=a^{-1}\epsilon^{-3/2}\quad\text{and}\quad\tau_{\beta^{\rm C}}(x_{\beta^{\rm C}})=a^{-1/4}(\beta^{\rm C})^{-3/4}. \tag{1b}$$

Since the curves for $\epsilon=10^{-7}$ to 10^{-5} are not clearly resolvable in the graph, we have not shown those curves, in order to avoid crowding. In models 1–4, the continuum processes control the FT. The positive maxima of the polarization profile occur for $x\le x_{\rm FT}$, where $x_{\rm FT}$ is defined as

$$x_{\rm FT}=\min[x_\epsilon,\,x_{\beta^{\rm C}}], \tag{2a}$$

with

$$x_\epsilon=\epsilon^{-1/2}\quad\text{and}\quad x_{\beta^{\rm C}}=(a/\beta^{\rm C})^{1/4}. \tag{2b}$$

The intensity source function $S_I(\tau)$ becomes depth-independent as $\epsilon\rightarrow 1$ (LTE case). The Q-source function $S_Q(\tau)$ tends to zero everywhere in the atmosphere. From Table 1 we can see that for models 3–6 the characteristic frequencies $x_{\rm PD}$ for photon destruction (PD), given by

$$x_{\rm PD}=\min[x_{\rm th},\,x_{\beta^{\rm C}}], \tag{3a}$$

with

$$x_{\rm th}=(a/\epsilon)^{1/3}\quad\text{and}\quad x_{\beta^{\rm C}}=(a/\beta^{\rm C})^{1/4}, \tag{3b}$$

are smaller than the corresponding values of $x_{\rm FT}$. Thus, for these models 3–6, the inelastic collisional random walk, which results in destruction and creation of photons, dominates over the redistributing multiple scattering process. However, for models 1 and 2 the multiple scattering process is still the important mode of line transfer.

The characteristic depth of PD, which is also called the thermalization length, is given by

$$\tau_{\rm PD}=\min[\tau_{\rm th}(x_{\rm th}),\quad\tau_{\beta^{\rm C}}(x_{\beta^{\rm C}})], \tag{4a}$$

with

$$\tau_{\rm th}(x_{\rm th})=1/\epsilon\quad\text{and}\quad\tau_{\beta^{\rm C}}(x_{\beta^{\rm C}})=a^{-1/4}(\beta^{\rm C})^{-3/4}. \tag{4b}$$

Since the collisions come to play an important role even in the shallow layers of the atmosphere, the models 3–6 show that the polarization gradually approaches zero even in the line core. All these models are also effectively thick ($\epsilon T^{\rm L}\gg 1$). The condition for the importance of PRD effects, $q=\pi^2\beta^{\rm C}/a\ll 1$, is satisfied by all the models. Further, the mean number of scatterings undergone by photons in the atmosphere is given by (Hummer & Kunasz 1980; Hubeny 1985a)

$$\langle N\rangle\sim\tau_{\beta^{\rm C}}(x_{\beta^{\rm C}})\sim a^{-1/4}(\beta^{\rm C})^{-3/4}, \tag{5}$$

and the mean path-length of photons, which is proportional to the mean time spent by photons in the medium (Ivanov

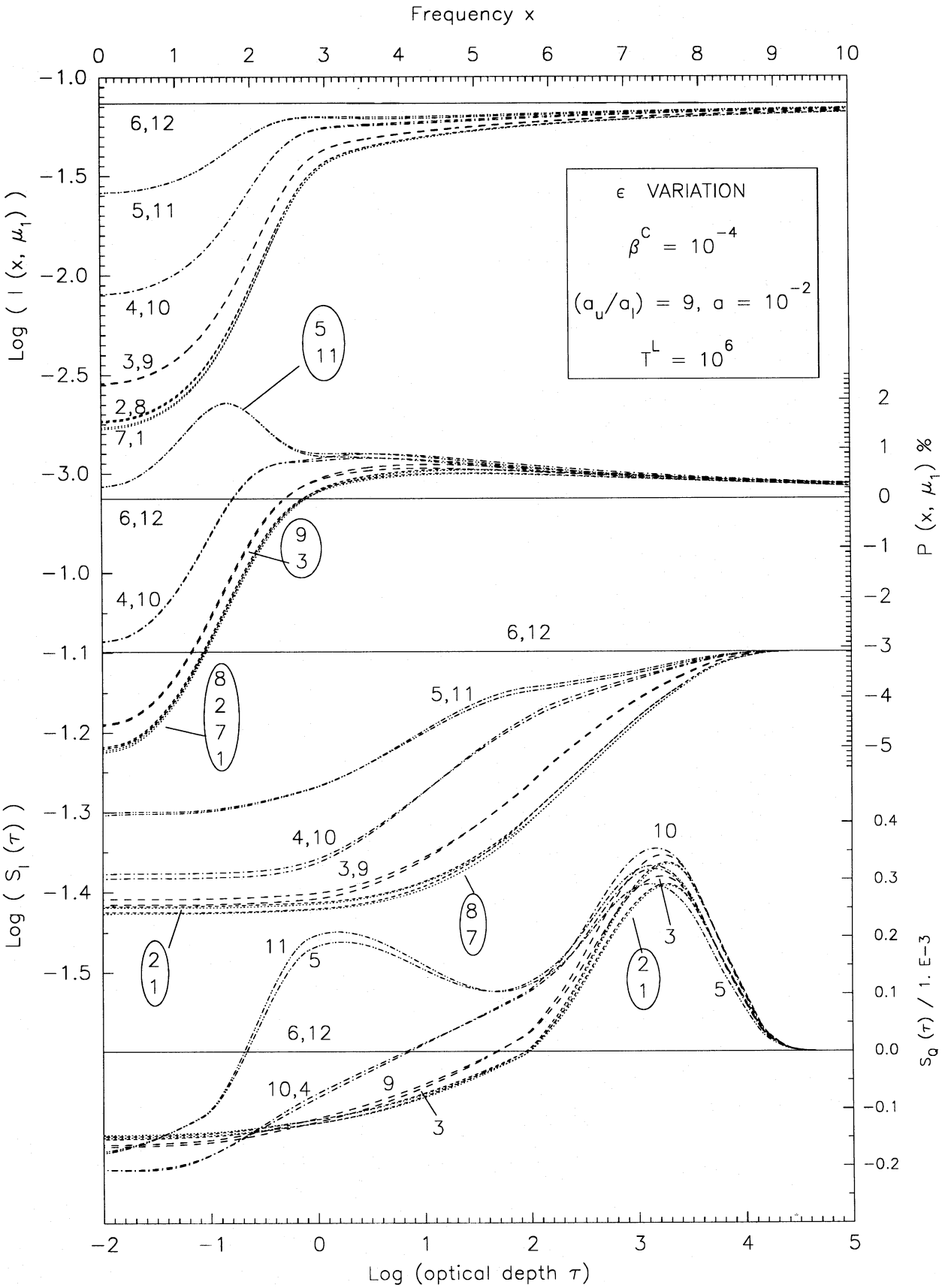

Figure 1. The effect of the thermalization parameter ϵ. Emergent intensity I and percentage polarization $p = (Q/I) \times 100$ in the direction $\mu = 0.11$ are shown in the first two panels. The abscissa for these two upper panels is the frequency x measured from line centre in units of a constant Doppler width. The model parameters are described in Section 2. Some of the global parameters (ϵ, β^C, a, T^L) are given inside the figure for easy reference. The lower two panels refer to the optical depth (τ) dependence of the intensity source function $S_I(\tau)$ and the polarized source function $S_Q(\tau)$. The abscissa for these two panels is log τ. The numbers shown near the curves identify models. Models 1–6 represent the resonance lines drawn as thin curves, and the models 7–12 the corresponding models for subordinate lines drawn as heavy curves. See Section 2.1 and Table 1 for further details.

Table 1. The effect of the thermalization parameter: ϵ: $T^{C}=10^{2}$; $T_{opt}=21.5$, $x_{\beta^C}=3.2$, $\tau_{\beta^C}=3.2\times10^{3}$, $x_{CS}=5.6$, $q=0.1$, $\langle N\rangle\simeq3.2\times10^{3}$, $\langle P\rangle\sim10^{-4}$, $\langle I\rangle\sim10^{4}$.

Model	ϵ	x_ϵ	τ_ϵ	x_{th}	τ_{th}	x_{FT}	τ_{FT}	x_{PD}	τ_{PD}	T_{eff}
							($\times10^{3}$)			
1	10^{-8}	10^{4}	10^{14}	10^{2}	10^{8}	3.2	3.2	3.2	3.2 10^{3}	10^{-2}
2	10^{-4}	10^{2}	10^{8}	4.6	10^{4}	3.2	3.2	3.2	3.2 10^{3}	10^{2}
3	10^{-3}	31.6	3.2 10^{6}	2.2	10^{3}	3.2	3.2	2.2	10^{3}	10^{3}
4	10^{-2}	10	10^{5}	1	10^{2}	3.2	3.2	1	10^{2}	10^{4}
5	10^{-1}	3.2	3.2 10^{3}	0.5	10	3.2	3.2	0.5	10	10^{5}
6	1	1	10^{2}	0.2	1	1	0.1	0.2	1	10^{6}

1970), is given by

$$\langle I\rangle\sim\frac{1}{\beta^{C}}. \tag{6}$$

For resonance lines formed by PRD as well as CRD, the mean escape probability is essentially not affected by the destruction processes. This probability is given by (see Frisch 1984)

$$\langle P\rangle=\frac{1}{1-\epsilon}\left[\frac{1}{\langle N\rangle}-\epsilon\right]\sim\frac{1}{\langle N\rangle}. \tag{7}$$

From Table 1 it can be clearly seen that, in spite of larger mean path-length, the medium is scattering-dominated, since it is optically thick $T_{opt}=(aT^{L})^{1/4}\gg1$. The ϵ parameter is directly related to the inelastic collisional rate Γ_I through a functional form

$$\Gamma_I(\epsilon)=\frac{\epsilon\Gamma_R}{(1-\epsilon)[1-\exp(-h\nu_0/kT_e)]}, \tag{8}$$

with the total damping parameter a that relates Γ_R, Γ_C and $\Delta\nu_D$ given by

$$a=\frac{\Gamma_R+\Gamma_C}{4\pi\Delta\nu_D} \tag{9}$$

in the conventional notation. Since we have selected a to be constant for all these models, it is implicit that the series of models presented in Fig. 1 directly show the effect of variation of inelastic collisions on the resonance and subordinate line formation (see equation 8).

2.2 The effect of continuous absorption parameter β^{C} on line polarization

The results of the computation are shown in Fig. 2 and Table 2. The variation of the continuum opacity affects the line intensity and polarization quite strongly. The intensity profiles become narrow and shallow as the β^{C} value is changed from 10^{-8} to 1. The values of β^{C} employed in these models are shown in Table 2. All the models in Fig. 2 are optically and effectively thick. However, the continuum optical depth $T^{C}=\beta^{C}T^{L}$ is different for different models. The characteristic frequency for frequency thermalization x_{FT} varies as an inverse fractional power of β^{C}. The quantity x_{FT} basically represents the frequency point at which the continuum radiation field begins to exceed the line radiation field. For $x<x_{FT}$ the line radiation field behaves as though β^{C} is effectively very small, irrespective of the actual value of β^{C} employed. Since x_{FT} becomes so small that it falls within the inner line core as $\beta^{C}\rightarrow1$, the intensity profiles are weakened. The position of the polarization wing maxima gradually shifts towards the line centre until finally the polarization is maximum only at the line centre for $\beta^{C}=1$. Secondly, the magnitude of polarization itself (irrespective of the sign) gradually decreases throughout the line profile as the β^{C} value is increased from 10^{-8} to 1.0. The global behaviour of the source function is controlled by $\tau_{PD}(x_{PD})$. Notice that for models 1 and 2 and models 8 and 9, for which $\epsilon>\beta^{C}$, we have $x_{PD}<x_{FT}$ and $\tau_{PD}(x_{PD})<\tau_{FT}(x_{FT})$. Hence, for these models, the collisional random walk is more important than the redistributing multiple scatterings. However, for models 4–7 and models 11–14, both these processes are equally important. In this respect $\beta^{C}\rightarrow1$ is quite different from the $\epsilon\rightarrow1$ situation shown previously in Table 1, where the PD by inelastic collisions (and thermal creation) are more important processes than multiple scattering, for $\epsilon>\beta^{C}$. Also note that for the combination of parameters we have selected, the subordinate lines do not greatly differ from the resonance lines, except when $\beta^{C}\leq10^{-8}$. The intensity source function $S_I(\tau)$ gradually increases in magnitude as β^{C} is increased, and finally becomes depth-independent for $\beta^{C}\rightarrow1$. The outward shift of maxima of $S_Q(\tau)$ and its transition from negative to positive values manifest themselves in the emergent polarization profiles. It is useful to note that beyond the frequency point

$$x_{CS}=(a/\pi\beta^{C})^{1/2}, \tag{10}$$

β^{C} dominates the total source function, and the residual PRD contribution represented by R_{II-A} can be considered as just coherent scattering (CS). The quantity x_{CS} depends strongly on β^{C}. From Table 2 we can see clearly that as $\beta^{C}\rightarrow1$ the R_{II-A} mechanism can be treated as coherent scattering almost throughout the line profile except close to line centre. This

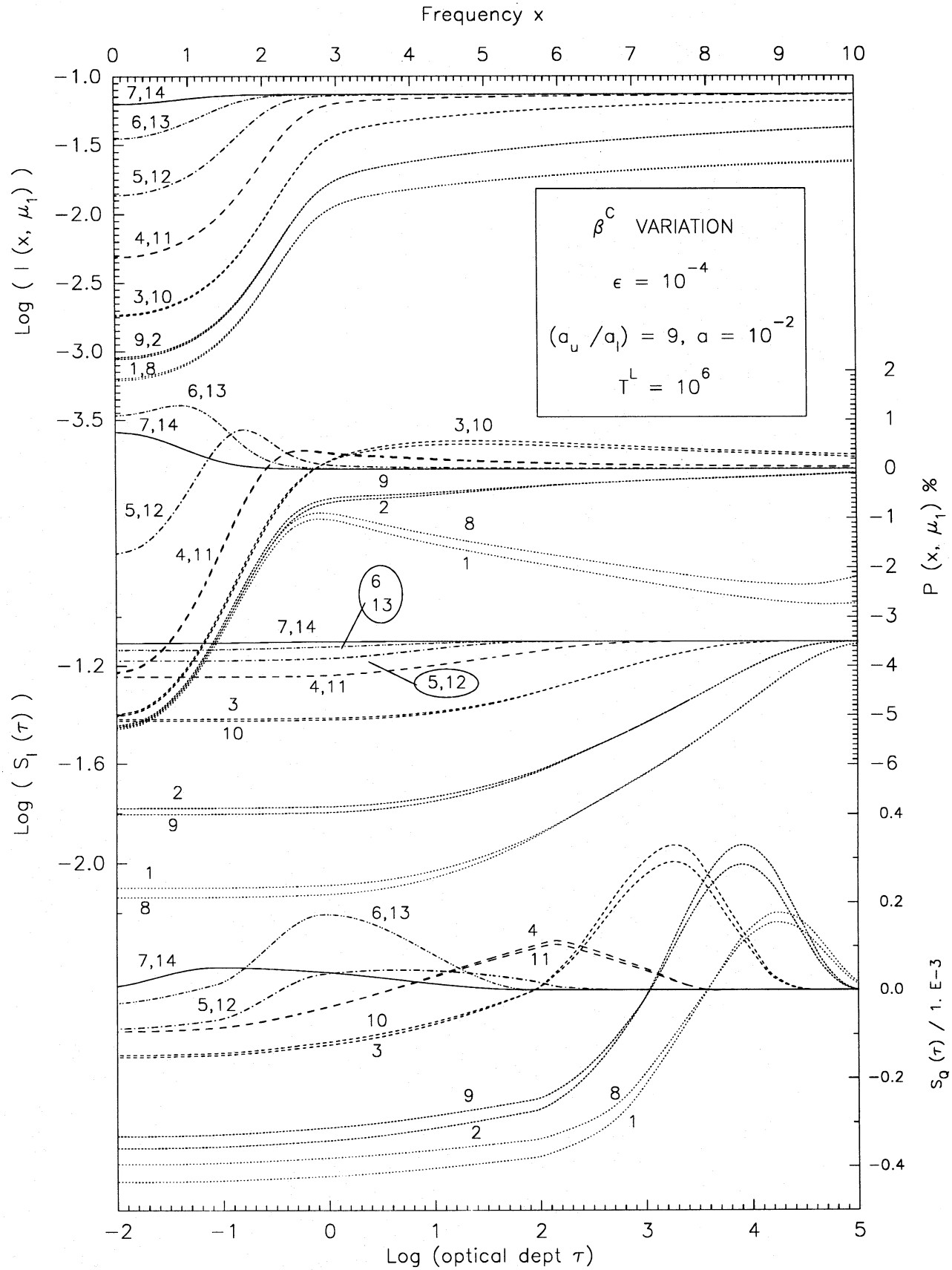

Figure 2. The effect of the continuous absorption parameter $\beta^C = k^C/k^L$. The quantities plotted are same as in Fig. 1. The mode of identifying the curves is also the same. Models 1–7 represent the resonance lines, and models 8–14 the subordinate lines. See Section 2.2 and Table 2 for a discussion of the models.

Table 2. The effect of the continuum absorption parameter β^C: $T_{\rm eff}=10^2$, $T_{\rm opt}=21.5$, $x_\epsilon=10^2$, $\tau_\epsilon=10^8$, $x_{\rm th}=4.6$, $\tau_{\rm th}=10^4$, $\langle N\rangle=\tau_{\beta^C}$.

Model	β^C	x_{β^C}	τ_{β^C}	x_{FT}	τ_{FT}	x_{PD}	τ_{PD}	x_{CS}	$<P>$	$<l>$	q	T^C
1	10^{-8}	31.6	$3.2\,10^6$	31.6	$3.2\,10^6$	4.6	10^4	564	$3.2\,10^{-7}$	10^8	10^{-5}	10^{-2}
2	10^{-5}	5.6	$1.8\,10^4$	5.6	$1.8\,10^4$	4.6	10^4	17.8	$5.6\,10^{-5}$	10^5	10^{-2}	10
3	10^{-4}	3.2	$3.2\,10^3$	3.2	$3.2\,10^3$	3.2	$3.2\,10^3$	5.6	$3.2\,10^{-4}$	10^4	10^{-1}	10^2
4	10^{-3}	1.8	$5.6\,10^2$	1.8	$5.6\,10^2$	1.8	$5.6\,10^2$	1.8	$1.8\,10^{-3}$	10^3	1	10^3
5	10^{-2}	1	10^2	1	10^2	1	10^2	0.6	$1.0\,10^{-2}$	10^2	10	10^4
6	10^{-1}	0.6	$1.8\,10^1$	0.6	$1.8\,10^1$	0.6	$1.8\,10^1$	0.2	$5.6\,10^{-2}$	10	10^2	10^5
7	1	0.3	3.2	0.3	3.2	0.3	3.2	0.06	$3.2\,10^{-1}$	1	10^3	10^6

fact may provide computational advantages in work related to model atmospheres, since real stellar atmospheres indeed have strong continuum absorption due to various sources. Notice that $\langle N\rangle$ also becomes extremely small, and that the escape probability is so high when $\beta^C=1$ that the whole atmosphere appears as an isothermal photosphere emitting continuum radiation even at line frequencies. Since $q\ll 1$ only for models 1–3 and models 8–10, the PRD effects are important only for these models. The rest of the models are dominated by the continuum absorption parameter β^C. Except for models 1 and 8, all the models are saturated, since the conditions $T^L\gg\tau_{\rm FT}(x_{\rm FT})$ and $T^L\gg\tau_{\rm PD}(x_{\rm PD})$ are simultaneously satisfied.

2.3 The effect of variation of average optical depth T^L on the line polarization

The series of models presented in Fig. 3 and Table 3 show the effect of variation of line optical depth T^L on the shape of intensity and polarization profiles. Models 1–4 represent the resonance lines, and models 5–8 the corresponding subordinate lines. All the models are optically and effectively thick. Since $\epsilon=\beta^C$ in our models, the effective thickness $T_{\rm eff}=\epsilon T^L$ is always equal to the continuum optical depth, $T^C=\beta^C T^L$. The PRD effects are important in all the models, since the condition $q\ll 1$ is satisfied for all of them. Since $x_{\rm PD}=x_{\rm FT}$ and $\tau_{\rm PD}=\tau_{\rm FT}$, the collisional random walk process is as significant as the multiple scattering process responsible for frequency diffusion of photons.

The cases 1 and 5 are somewhat different from others, since for these two cases $T_{\rm eff}=T_{\rm opt}=T^C$. The polarization remains negative throughout the line profile for these two cases. The intensity profiles for the model pairs (2, 6), (3, 7) and (4, 8) do not differ much from each other. However, the wing polarization profiles (2, 6), (3, 4) and (7, 8) form pairs. In general, the subordinate line polarizations are slightly smaller than the corresponding resonance line polarizations. Notice, however, the strong dependence of $S_I(\tau)$ and $S_Q(\tau)$ on the optical depth T^L. The resonance line and subordinate line cases go as pairs, for each value of T^L, with only small differences in values of the source functions. As the value of T^L is increased from 10^5 to 10^8, the saturation point of the $S_I(\tau)$ moves outwards. The saturation point may be defined as the depth at which $S_I(\tau)\rightarrow$ constant $\times B$. This outward shift is obviously due to the occurrence of higher optical depths in the outer layers, as T^L is increased. The optical depth scales are computed using a $k^L(r)=kr^{-2}$ type variation of opacity. Irrespective of the increase in total optical depth, the escape factors $\langle N\rangle$, $\langle P\rangle$ and $\langle l\rangle$ remain constant for our models. Although the profiles of effectively thin ($\epsilon T^L\ll 1$) and effectively thick ($\epsilon T^L\gg 1$) atmospheres differ significantly, the difference among optically thick emergent profiles themselves is only marginal.

2.4 The effect of variation damping parameter a on line polarization

The results of the computation for this series of models are shown in Fig. 4 and Table 4. Variation of a is equivalent to variation of radiative damping width Γ_R in our models (see equation 9). All the models in this figure are optically and effectively thick ($\epsilon T^L=10^2$ and $(aT^L)^{1/3}\gg 1$). From Table 4 it can also be seen that all these models are controlled by the parameter β^C, and consequently the frequency thermalization (FT) occurs due to multiple scattering of diffuse radiation field in the atmosphere. A strong damping of the wings of intensity profiles occurs as the value of a increases. The polarization profiles also become wider. More importantly, the crossover point from negative to positive polarization moves out into the wings as a is increased. Except for the pair of models (1, 6), for which the PRD effects are not important ($q>1$), the crossover frequency is approximately given by $x_{\rm FT}$. The frequency of transition $x_{\rm CS}$ to the coherent regime moves out into the wings as a is increased. However, $\langle N\rangle$ and $\langle P\rangle$ have an interesting behaviour, with $\langle N\rangle$ showing a minimum for a certain value of a. Correspondingly, the mean escape probability $\langle P\rangle$ shows the inverse of this behaviour (see Table 4). The source function $S_I(\tau)$ decreases strongly throughout the outer atmosphere as the damping parameter a is increased. The polarized source function $S_Q(\tau)$ shows a corresponding increase for depths $\tau<T^C$. However, $S_Q(\tau)$ maxima that generally occur in the region $T^C<\tau<10^4$ in the frequency-thermalized models undergo a shift from larger to smaller values of τ as the damping parameter a is increased. There is some difference between the behaviour of resonance and subordinate line $S_Q(\tau)$ source functions in this range of optical depths.

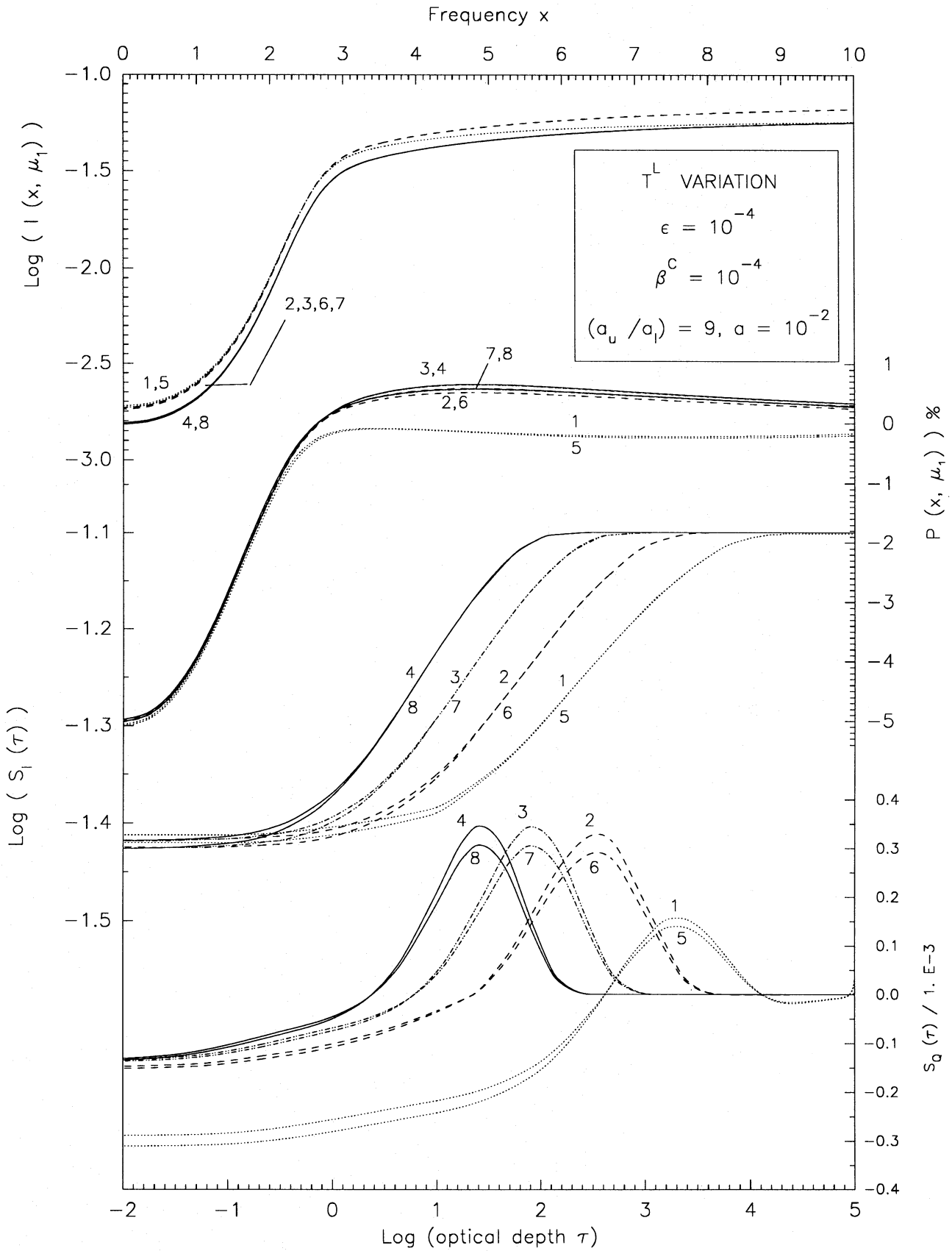

Figure 3. The effect of the optical depth parameter T^L. Models 1–4 represent the resonance lines, and models 5–8 the subordinate lines. See Section 2.3 and Table 3 for further details.

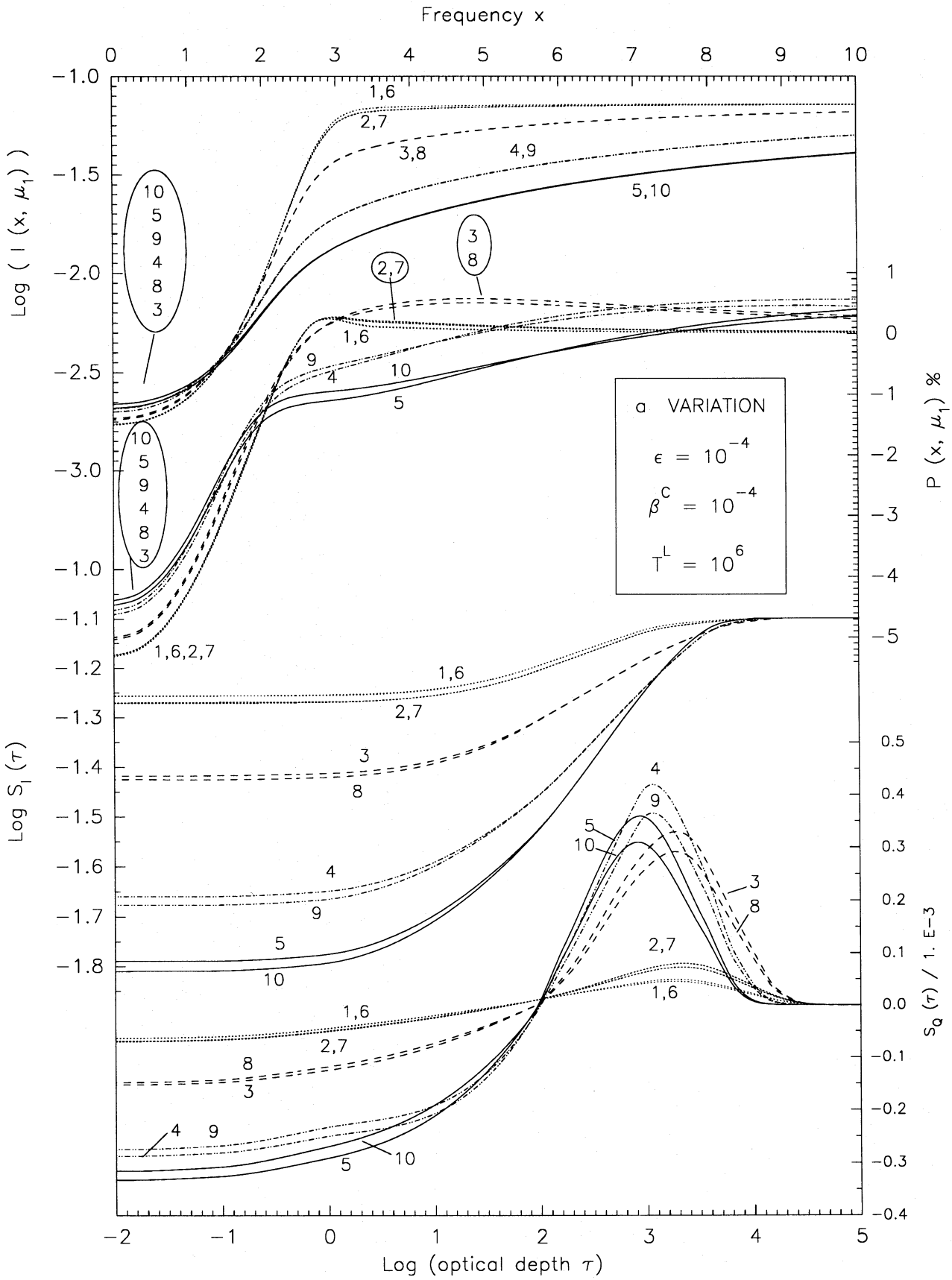

Figure 4. The effect of the damping parameter *a*. Models 1–5 represent the resonance lines, and models 6–10 the subordinate lines. See Section 2.4 and Table 4 for further details.

Table 3. The effect of the optical depth parameter T^L: $x_\epsilon = 10^2$, $\tau_\epsilon = 10^8$, $x_{\beta^C} = 3.2$, $\tau_{\beta^C} = 3.2 \times 10^3$, $x_{CS} = 5.6$, $x_{th} = 4.6$, $\tau_{th} = 10^4$, $q = 0.1$, $\langle N \rangle \simeq 3.2 \times 10^3$, $\langle P \rangle \sim 3.2 \times 10^{-4}$, $\langle I \rangle \sim 10^4$, $x_{PD} = x_{FT}$, $\tau_{PD} = \tau_{FT}$.

Model	T^L	T_{eff}	T^C	T_{opt}	x_{FT}	τ_{FT} $\times 10^3$
1	10^5	10	10	10	3.2	3.2
2	10^6	10^2	10^2	21.5	3.2	3.2
3	10^7	10^3	10^3	46.4	3.2	3.2
4	10^8	10^4	10^4	100	3.2	3.2

Table 4. The effect of the damping parameter a: $T_{eff} = 10^2$, $T^C = 10^2$, $x_\epsilon = 10^2$, $\tau_\epsilon = 10^8$, $\tau_{th} = 10^4$, $\langle N \rangle \simeq \tau_{\beta^C}$, $\langle I \rangle \sim 10^4$, $x_{PD} = x_{FT}$, $\tau_{PD} = \tau_{FT}$.

Model	a	x_{th}	x_{β^C}	τ_{β^C}	x_{FT}	τ_{FT}	x_{CS}	$< P >$	q	T_{opt}
1	$5\ 10^{-4}$	1.7	1.5	$6.7\ 10^3$	1.5	$6.7\ 10^3$	1.3	$1.5\ 10^{-4}$	2.0	7.9
2	10^{-3}	2.2	1.8	$5.6\ 10^3$	1.8	$5.6\ 10^3$	1.8	$1.8\ 10^{-4}$	1.0	10
3	10^{-2}	4.6	3.2	$3.2\ 10^2$	3.2	$3.2\ 10^2$	5.6	$3.2\ 10^{-3}$	0.1	21.5
4	$5\ 10^{-2}$	7.9	4.7	$4.7\ 10^2$	4.7	$4.7\ 10^2$	12.6	$2.1\ 10^{-3}$	0.02	36.8
5	10^{-1}	10	5.6	$5.6\ 10^2$	5.6	$5.6\ 10^2$	17.8	$1.8\ 10^{-3}$	0.01	46.4

2.5 The effect of branching ratio Λ on line polarization

Following Omont, Smith & Cooper (1972) and Hubeny & Heinzel (1984), we can include the collisional redistribution effects in resonance lines through the equation

$$R_A(x, x') = \Lambda R_{II-A}(x, x') + (1-\Lambda) R_{III-A}(x, x'), \quad (11)$$

and in subordinate lines through the equation

$$R_A(x, x') = \Lambda R_{V-A}(x, x') + (1-\Lambda) R_{III-A}(x, x'). \quad (12)$$

The factor Λ which represented the degree of non-coherence is called the branching ratio. It is given by the expression

$$\Lambda = \frac{\Gamma_R + \Gamma_I}{\Gamma_R + \Gamma_I + Q_E}, \quad (13)$$

where Γ_R, Γ_I and Q_E are the radiative, inelastic and elastic collisional widths. The results are presented in Fig. 5 and Table 5. The curves 1 and 7 represent the pure R_{III-A} case. There is no significant difference between the profiles corresponding to (R_{II-A}, R_{III-A}) combination and (R_{V-A}, R_{III-A}) combination, for almost all values of Λ. However, pure R_{II-A} and R_{III-A} cases are distinctly different from the combination cases, as is clearly seen through the depth dependence of S_I and S_Q source functions. All the models in Fig. 5 are controlled by PRD effects, since $q \ll 1$. These models show a transition from negative to positive polarization within the line core, and the transition frequency is roughly given by x_{FT}. Further, τ_{FT} gives the position of the $S_Q(\tau)$ peaks for all these models. The polarization profiles reach a positive maximum roughly around $x \simeq x_{th}$. Fig. 5 also shows that the R_{II-A} scaling laws can be generally used even for other redistribution functions, particularly when there is a strong continuum, as in our models. Notice the similarity in emergent profiles between the R_{V-A} redistribution, with its twin emission probability at core and wing, and the R_{II-A} redistribution. The fact that R_{II-A} and R_{V-A} themselves can be expressed as a linear combination of CRD and CS shows that the partial coherent scattering (PCS) approximation, particularly its variant involving a depth-dependent division frequency between the CRD-type core and the CS-type wing redistribution (see Hubeny 1985a,b), provides a valid approximation for dealing practically with (R_{II-A}, R_{III-A}) and (R_{V-A}, R_{III-A}) combinations.

2.6 The effect of sphericity parameter *R* on line polarization

The characteristics of line transfer in SS systems is discussed in great detail by Kunasz & Hummer (1974). The characteristics of resonance line polarization in SS systems is discussed in Nagendra (1988). In Fig. 6 and Table 6 we discuss the peculiarities of resonance line polarization in spherical atmospheres with large radial extent. There are three characteristics which constitute the so-called curvature effect caused by large radial extent. They are the 'bias' in scattering towards larger radius, the 'dilution' of the diffuse radiation field, and the 'peaking' of the radiation towards radial direction. The case 1 shown by dotted lines corresponds to a plane-parallel atmosphere. The dilution of mean intensity J for departures from planar limit is given by

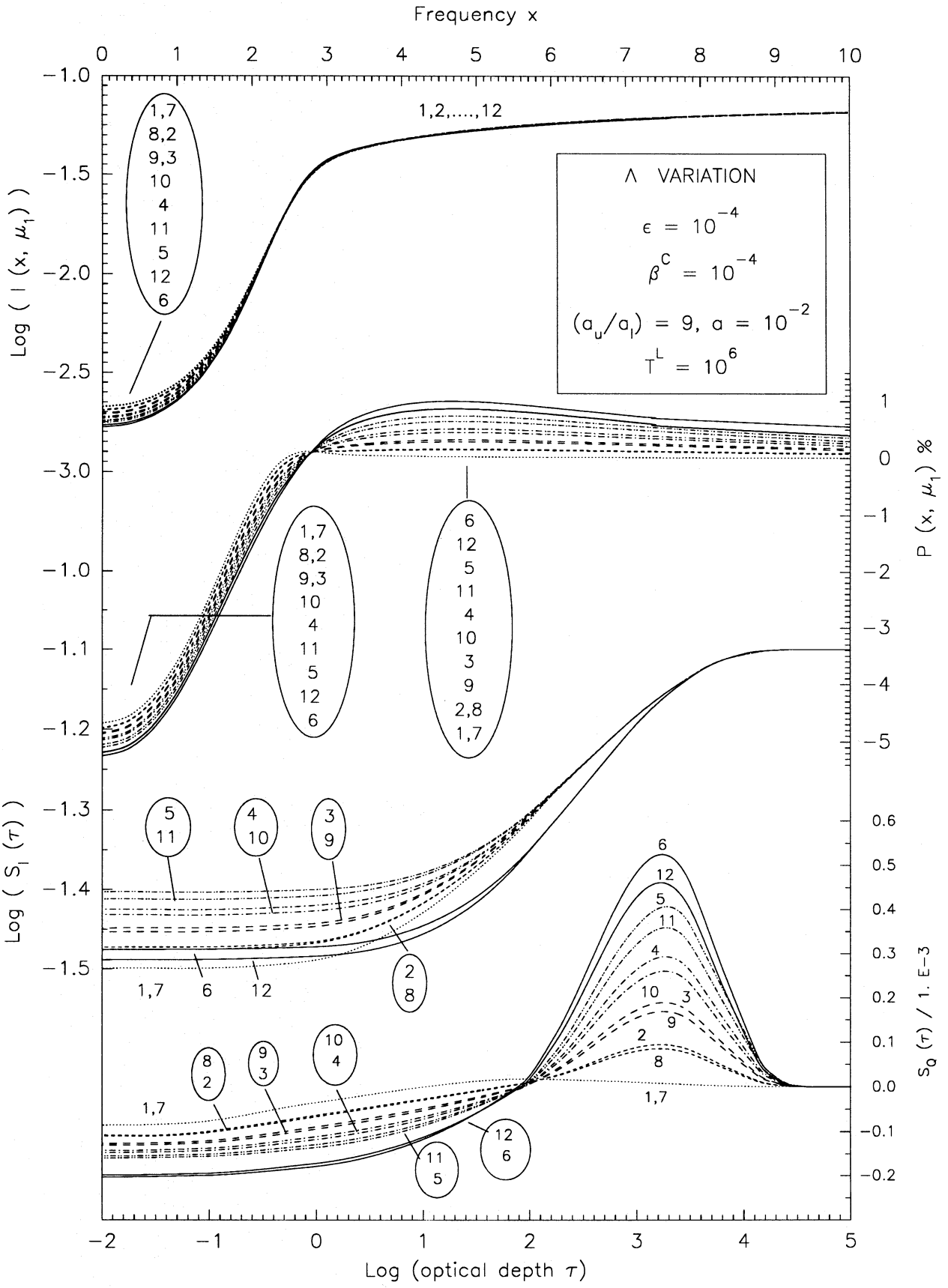

Figure 5. The effect of the branching ratio Λ. Models 1–6 show the collisional effects on resonance lines, and models 7–12 represent the corresponding effects on subordinate lines. See Section 2.5 and Table 5 for further details.

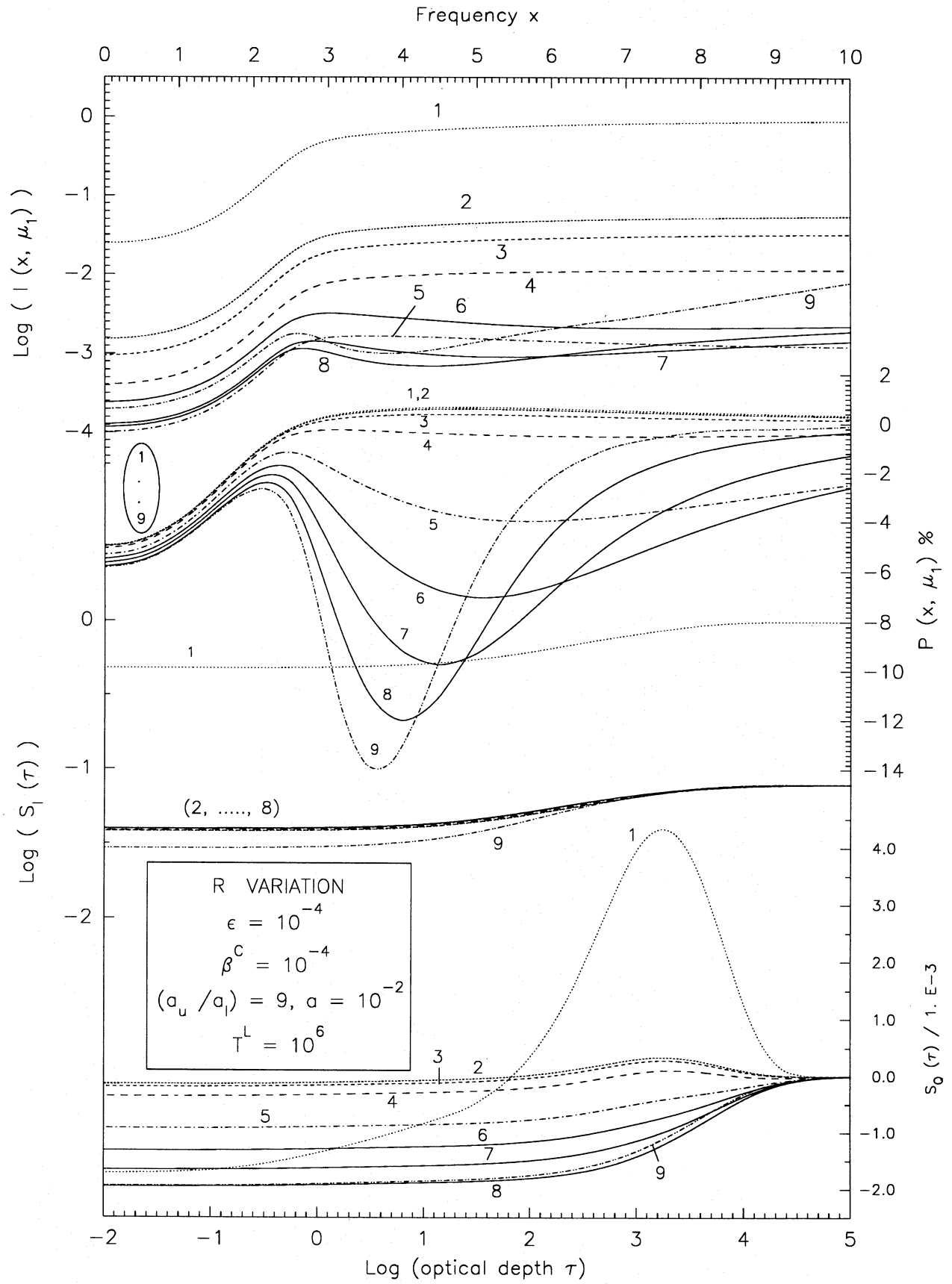

Figure 6. The effect of the radial extent R of the spherical shell atmosphere. The model 1 shows the results for a plane-parallel atmosphere, and models 2–9 represent the spherical atmospheres. See Section 2.6 and Table 6 for further details.

Table 5. The effect of the branching ratio Λ: $T^{C}=10^{2}$, $T_{opt}=21.5$, $T_{eff}=10^{2}$, $x_{\epsilon}=10^{2}$, $\tau_{\epsilon}=10^{8}$, $x_{\beta c}=3.2$, $\tau_{\beta c}=3.2\times10^{3}$, $x_{CS}=5.6$, $q=0.1$, $\langle N\rangle\simeq3.2\times10^{3}$, $\langle P\rangle\sim3.2\times10^{-4}$, $\langle l\rangle\sim10^{4}$, $x_{PD}=x_{FT}$, $\tau_{PD}=\tau_{FT}$.

Model	Λ	x_{th}	τ_{th}	x_{FT}	τ_{FT} $\times10^{3}$
1	0.0	10^{2}	10^{6}	3.2	3.2
2	0.2	4.6	10^{4}	3.2	3.2
3	0.4	4.6	10^{4}	3.2	3.2
4	0.6	4.6	10^{4}	3.2	3.2
5	0.8	4.6	10^{4}	3.2	3.2
6	1.0	4.6	10^{4}	3.2	3.2

$$W=0.5\,J(R)/J(R=1)=0.5[1-(1-1/R^{2})^{1/2}]. \quad (14)$$

This factor W is listed in Table 6. The spherical dilution comes into the picture mainly in regions of the atmosphere where a ray traverses large volumes of space without a significant probability of interacting with matter, namely in the outermost layers of the atmosphere where $\tau\ll1$. For the models shown in Fig. 6 (particularly those with a large outer radius, $R\gg1$), only a small portion of the atmosphere is optically thin ($\tau\ll1$) at all frequencies. The radius r_1 at which the mean optical depth $\tau=1$ occurs is given by

$$(r_1/R)=(T^{L})^{1/n-1}[T^{L}-1+(R/R_{C})^{n-1}]^{1/n-1} \quad (15)$$

(see Kunasz & Hummer 1974). In our models, $n=2$ and $R_{C}=1$. Since we employ a large value of T^{L}, all the models in Fig. 6 have $(r_1/R)\approx1$. The emergent intensity $I(x,\mu_1)$ changes only by a factor of 20 as we go from $R=3$ to a large value of outer radius, $R=243$. This relatively smaller change is due to the presence of a strong continuum emission throughout the medium. The wing polarization gradually increases in magnitude as R is increased. For $R=81$, a broad negative polarization trough is formed. As R increases further, the maxima of the negative polarization troughs shift towards the line core and the troughs become narrow, increasing in magnitude at the same time. They are related to the mid-wing absorption troughs in the intensity profile. A differential measure of the dilution effect at any frequency point x in the line is given by

$$e(x)=R/r_1(x)=[T^{L}(x)-1+(R/R_{C})^{n-1}]^{1/n-1}/[T^{L}(x)]^{1/n-1}, \quad (16)$$

where $T^{L}(x)=T^{L}\phi(x)$. If $e(x)\sim1$, the dilution effects are small, but if $e(x)\gg1$, they are important. We can easily verify that the dilution effects are quite significant for all the models 2–9 for frequencies $x>2$, which means that the line-wing photons can traverse larger and larger spherical volumes of outer atmosphere, as the radial extent R is increased, with only a small probability of interacting with matter. Such long mean free paths have direct consequences on the escape of photons in the line wings. For $r\ll r_1(x)$, the intensity at frequency x will be essentially isotropic, and its dependence on radius will be determined by diffuse radiation at all other frequencies. For $r\gg r_1(x)$, the emergent intensity will be strongly forward-peaked. When the dilution becomes significant, mainly in systems with large R, the angular width of this radially directed peak is given approximately by $1/e(x)$. A detailed discussion of the frequency dependence of $e(x)$, and its contribution to deviations from isotropy (Eddington factor), as a function of depth, is presented by Kunasz & Hummer (1974). We find that spherical dilution can partially explain the occurrence of mid-wing polarization peaks, and their frequency dependence.

Table 6. The effect of variation of the radial extent R: $T^{C}=10^{2}$, $T_{opt}=21.5$, $T_{eff}=10^{2}$, $x_{\epsilon}=10^{2}$, $\tau_{\epsilon}=10^{8}$, $x_{\beta c}=3.2$, $\tau_{\beta c}=3.2\times10^{3}$, $x_{CS}=5.6$, $q=0.1$, $\langle N\rangle\simeq3.2\times10^{3}$, $\langle P\rangle\sim3.2\times10^{-4}$, $\langle l\rangle\sim10^{4}$, $x_{PD}=x_{FT}$, $\tau_{PD}=\tau_{FT}$, $(r_1/R)=T^{L}/(T^{L}-1+R)\simeq1$, $W=0.5[1-(1-1/R^{2})^{1/2}]$.

Model	R	W
1	1	0.5
2	3	$2.86\ 10^{-2}$
3	9	$3.10\ 10^{-3}$
4	27	$3.43\ 10^{-4}$
5	81	$3.81\ 10^{-5}$
6	122	$1.68\ 10^{-5}$
7	162	$0.95\ 10^{-5}$
8	203	$0.61\ 10^{-5}$
9	243	$0.42\ 10^{-5}$

The bias in the scattering of photons preferentially to larger radii more often than to smaller radii is basic to spherical systems. For power-law opacities, the bias at radius r for scattering towards larger radii is defined as

$$\rho(r)=\omega_2(r)/\omega_1(r), \quad \text{with} \quad \omega_2(r)=1-\omega_1(r), \quad (17)$$

where $\omega_1(r)$ is the probability that a photon emitted with a frequency distribution $\phi(x)$ ends its flight within the sphere of radius r. Then $\omega_2(r)$ is the probability that the photon ends its flight at a radius larger than r. From table 2 of Kunasz & Hummer (1974) it is clearly seen that, for the R and T^{L} values that we are concerned in this paper, $\rho(r)\simeq1$ throughout the atmosphere for our models, which means that the scattering probability is nearly isotropic as in the case of PP

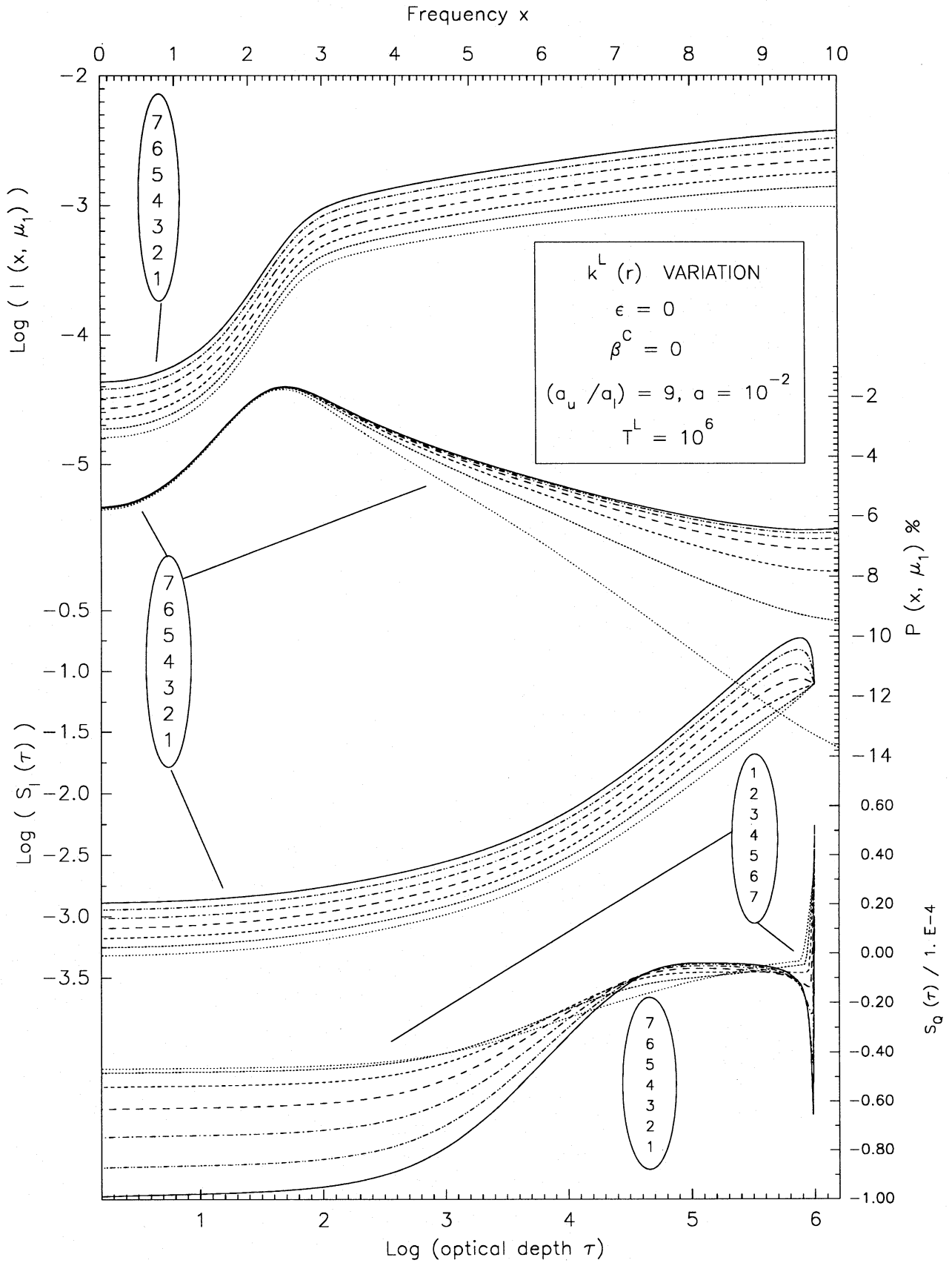

Figure 7. The effect of the power-law opacity $k^{L}(r)$ variation in spherical atmospheres on resonance lines. See Section 2.7 and Table 7 for details. Notice that a conservative scattering atmospheric model is employed for this figure.

layers. When this bias is important, i.e. $\rho(r) \gg 1$, the escape probability arguments become unreliable due to the outward drift of photons in SS systems. Since this bias is very weak in our models, we can continue to use escape probability expressions derived for PP atmospheres for rough estimates in SS systems also. The peaking of the radiation field arises when the medium is optically thin and photons emitted at smaller radii arrive at larger radii with single long flights. The ratio of the angles subtended by any ray with local radii at any two radial points r_1 and r_2 is given by

$$(1-\mu_{r_1}^2)^{1/2}/(1-\mu_{r_2}^2)^{1/2} = r_2/r_1, \quad \text{with} \quad \mu_{r_1} = \cos\theta_{r_1}$$
$$\text{and} \quad \mu_{r_2} = \cos\theta_{r_2}, \tag{18}$$

which shows that a ray subtends progressively smaller and smaller angles with local radii as it travels outwards without changing direction. Even this mechanism affects our emergent profiles only moderately, except in outer shallow layers where monochromatic line optical thicknesses are smaller. The angular narrowing of radiation field (see equation 18) is strong in a large-R atmosphere. The presence of the $(1-\mu^2)/r$ term with angle derivative of the SS transfer equation basically leads to a non-local mixing of quite different limb-darkened radiation fields, at any given radial point. This peaking of specific intensity in SS systems, referred to as curvature scattering, is also partially responsible for polarization troughs in the mid-wing frequency region.

2.7 The effect of power-law opacity variation on resonance line polarization

In Fig. 7 and Table 7 we show the effect of variation of index n of the power-law opacity $k(r) = K_n r^n$ on the formation of a resonance line with $\Lambda = 2/3$. We have employed a conservative scattering spherical shell ($\epsilon = \beta^C = 0$) for this series of models. The power-law variation of opacity in the 'standard model' does not produce a significant difference in the frequency dependence of polarization profiles, as compared to the usual results computed for an inverse-square law. It is due to the confinement of sharp changes in power-law opacity only close to the central core, where the diffuse radiation field is highly isotropic. For this reason, we have chosen an extreme model of conservative scattering, where interesting changes occur in the polarization profiles. The asymptotic scaling laws, for conservative scattering under Voigt CRD as well as for R_{II-A}, are given by Frisch (1988). As with other sections in this paper, we have employed the expressions relevant to R_{II-A} here also, for the sake of uniformity, and since R_{II-A} is overweighted compared to R_{III-A}, in the collisional redistribution. For conservative scattering, the characteristic frequency and characteristic depth are computed using $x_{PD} = x_{th} = (aT^L)^{1/3}$ and $\tau_{PD} = \tau_{th}(x_{th}) = T^L$. The mean number of scatterings and the mean path-length are computed from $\langle N \rangle = T^L$ and $\langle l \rangle = T^L(aT^L)^{1/3}$, respectively. The scaling constant K_n and the expressions for $\tau_n^L(r)$ are listed in Table 7. As n varies from -3 to $+3$, the intensity profiles gradually become weak and shallow throughout the bandwidth. The polarization in the line core is not affected, since both $S_I(\tau)$ and $S_Q(\tau)$ undergo a proportional change in those parts of the atmosphere where the line core is formed. However, in the deepest layers ($\log \tau > 4$), where the far wings of the lines are formed, the polarization rate $S_Q(\tau)/S_I(\tau)$ differs strongly for different values of n. As a result, the far-wing ($x > 6$) polarization is quite sensitive to n. Two important aspects of polarization profiles are that the polarization at $x \sim 10$ is larger than the core polarization, and that the polarization is fully negative in the entire line profile. The reason for this behaviour is the highly non-local nature of diffuse radiation field ($\epsilon = 0$) and a lack of coupling to the local anisotropy ($\beta_C = 0$) in the medium. The large polarization observed in the far-wing, for steeply varying opacity laws ($n = -3$ and $n = -2$), is caused by a concentration of opacity in the innermost layers, where the source function $S_I(\tau)$ gradient is large, resulting in a large number of scatterings. In a conservative scattering atmosphere, the polarization can reach zero level only far out in the wings, after undergoing negative maxima in the region $10 < x < 20$. The sharp variation in $S_Q(\tau)$ near the lower boundary is not unexpected, since the medium is highly scattering and the absence of continuum absorption provides a smooth transition of the internal radiation field to the Schuster boundary condition. It is clear from the polarization curves that, whereas the presence of near-wing maxima within the line core is basic to PRD line transfer, the sign change is not. The sign change seems to be related to the

Table 7. The effect of variation of the opacity index n: $T^C = 0$, $T_{opt} = 21.5$, $T_{eff} = 0$, $q = 0$, $x_{PD} = 21.5$, $\tau_{PD} = 10^6$, $\langle N \rangle \simeq 10^6$, $\langle P \rangle \simeq 10^{-4}$, $\langle l \rangle \simeq 21.5 \times 10^6$, $k_n^L(r) = K_n r^n$, $\tau_n^L(r) = K_n f(r)$, $r_1(x) = R\{\tau(x)/[\tau(x) - 1 + R^{n-1}]\}^{1/(n-1)}$, $e(x) = R/r_1(x)$.

Model	n	K_n	$f(r)$	$e(x = 10)$
1	-3	$2R^2T^L/(R^2-1)$	$0.5[1/r^2 - 1/R^2]$	1.008
2	-2	$RT^L/(R-1)$	$[1/r - 1/R]$	1.010
3	-1	T^L/lnR	$[lnR - lnr]$	1.014
4	$+0$	$T^L/(R-1)$	$[R - r]$	1.021
5	$+1$	$2T^L/(R^2-1)$	$0.5[R^2 - r^2]$	1.000
6	$+2$	$3T^L/(R^3-1)$	$(1/3)[R^3 - r^3]$	1.062
7	$+3$	$4T^L/(R^4-1)$	$(1/4)[R^4 - r^4]$	1.120

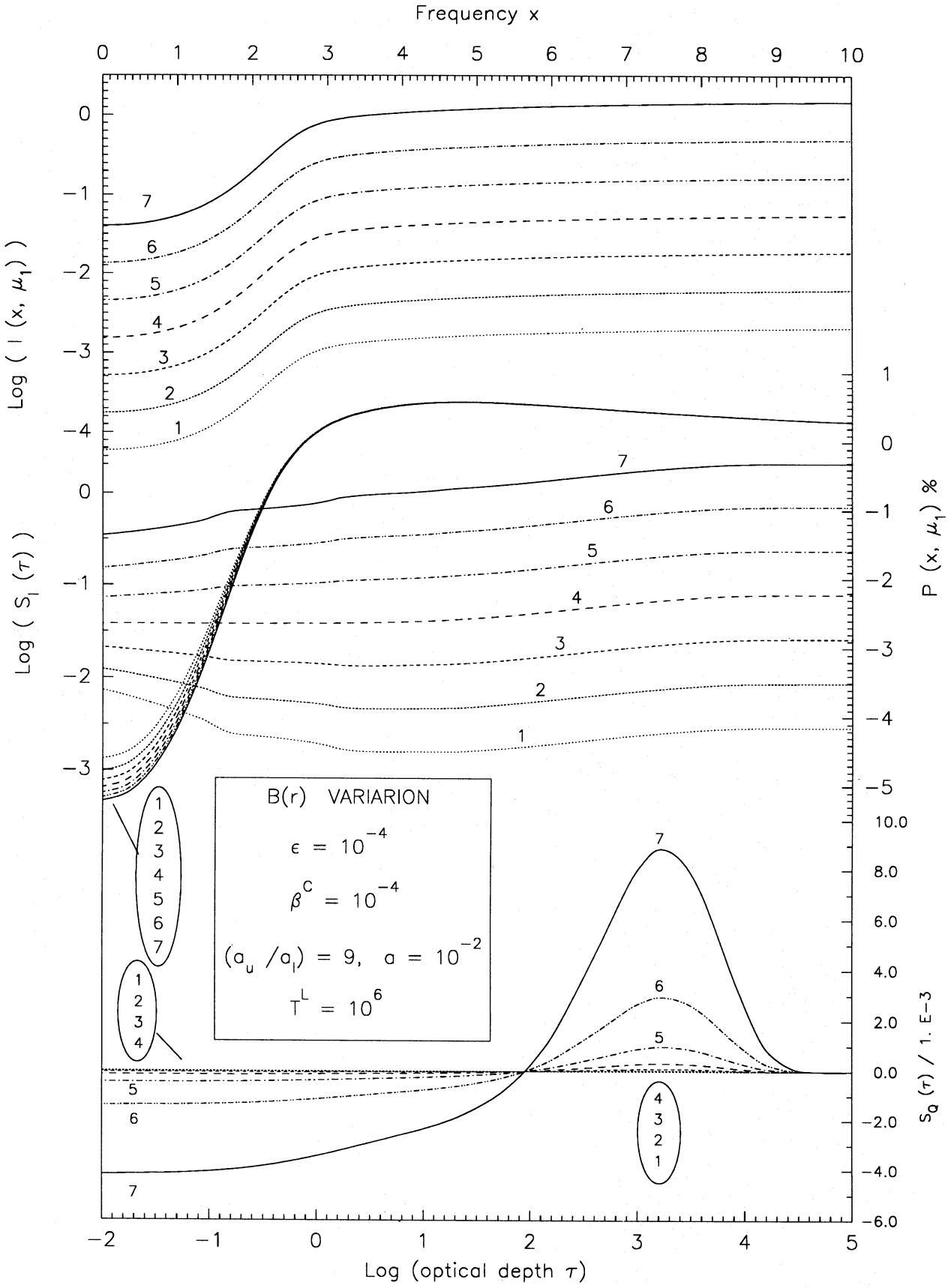

Figure 8. The effect of the power-law Planck function $B(r)$ variation in spherical atmospheres on resonance lines. See Section 2.8 and Table 8 for a discussion.

magnitude of unpolarized continuum radiation. In these models, the dilution as well as the bias is weak. Hence the changes observed are primarily due to changes in the opacity index.

2.8 The effect of power-law Planck function $B(r)$ variation on resonance line polarization

In Fig. 8 and Table 8 we show the effect of variation of index m, in the power-law variation of Planck function $B(r)=B_0 r^m$. As the index m changes from -3 to $+3$, the relative intensity of the entire profile increases proportionally. This happens because of the overall increase in the background continuum emission intensity in the line-forming region as we increase m, in the atmosphere which always has an inverse-square variation of opacity. The only perceptible change in polarization profile occurs near the line centre, which implies a relative insensitivity of the scattering part of the line source function to changes in the depth variation of isotropic emission, represented by $\epsilon B(r)$. For this same reason, the emergent polarization depends on the gradient of the scattering part of the source function and the gradient of $S_Q(\tau)$, rather than the gradient of $B(r)$ (see Table 8). Although $S_Q(\tau)$ for $\tau<10^5$ shows a strong dependence on m, it is not reflected equally strongly in the emergent line-wing polarization, which is insensitive to variation of m.

2.9 The effect of variation of collisional parameters in the Domke–Hubeny polarized redistribution matrix for resonance line polarization

In this section, we study the changes in the frequency dependence of resonance line polarization for an arbitrary variation of collisional parameters. We employ the general DH redistribution matrix (Domke & Hubeny 1988) to include the effects of collisions. This matrix depends explicitly on various channels of collisional redistribution, namely phase-changing elastic collisions ($\Gamma_C=Q_E$), inelastic collisions (Γ_I), and alignment-changing elastic collisions [$D^{(2)}$]. We have parametrized the variation of all these collision rates and the radiative damping rate (Γ_R). The parameters that remain the same for all these models are the damping constant, a, and the Doppler width,

$$\Delta\nu_D=(\nu_0/c)\sqrt{2kT_e/M^a},$$

for a line of central wavelength $\lambda_0=5000$ Å, formed in an isothermal atmosphere with $T_e=5000$ K. We parametrize the variation of Γ_C, Γ_I, $D^{(2)}$ and Γ_R through a variation of the free parameter f in the following set of equations:

$$\Gamma_R=f\Delta\nu_D, \tag{19a}$$

$$\Gamma_C=4\pi a\Delta\nu_D-\Gamma_R, \tag{19b}$$

$$D^{(2)}=0.379\Gamma_C \tag{19c}$$

and

$$\Gamma_I=\frac{\epsilon'\Gamma_R}{1-\exp(-h\nu_0/kT_e)}, \quad \text{with} \quad \epsilon'=\frac{\epsilon}{1-\epsilon}. \tag{19d}$$

The Doppler width $\Delta\nu_D=0.29\times10^{10}$ Hz and $a=10^{-2}$ for the present set of models. The expression for the angle-dependent redistribution matrix is given in Domke & Hubeny (1988). We have employed the angle-averaged version of that matrix, which can be obtained by using the angle–frequency separation according to Rees & Saliba (1982), as shown in Faurobert-Scholl (1991). It turns out that even the general DH redistribution function can be written formally as

$$R_{DH}=C_1[R_{II}(\text{anisotropic})]+C_2[R_{II}(\text{isotropic})]+C_3[R_{III}(\text{anisotropic})]+C_4[R_{III}(\text{isotropic})], \tag{20}$$

where the terms 'anisotropic' and 'isotropic' refer to the angular phase matrices involved in the scattering process, whose explicit forms are given in Domke & Hubeny (1988). The C coefficients are given in terms of the collisional branching ratios $\overline{\alpha}$, $\overline{\beta}^{(0)}$ and $\overline{\beta}^{(2)}$ as follows (see also Nagendra 1994):

$$C_1=W_2\overline{\alpha}=W_2\frac{\Gamma_R+\Gamma_I}{\Gamma_R+\Gamma_I+\Gamma_C}, \tag{21a}$$

$$C_2=(1-W_2)\overline{\alpha}=(1-W_2)\frac{\Gamma_R+\Gamma_I}{\Gamma_R+\Gamma_I+\Gamma_C}, \tag{21b}$$

$$C_3=W_2\overline{\beta}^{(2)}=W_2\left(\frac{\Gamma_R+\Gamma_I}{\Gamma_R+\Gamma_I+\Gamma_C}\right)\left(\frac{\Gamma_C-D^{(2)}}{\Gamma_R+\Gamma_I+D^{(2)}}\right), \tag{21c}$$

$$C_4=(\overline{\beta}^{(0)}-W_2\overline{\beta}^{(2)})=\left(\frac{\Gamma_C}{\Gamma_R+\Gamma_I+\Gamma_C}-C_3\right), \tag{21d}$$

which satisfy the normalization condition

$$C_1+C_2+C_3+C_4=1 \tag{21e}$$

in the conventional notation. In all the models we have selected the depolarization constant $W_2=0.9$. The actual physical significance of the branching ratios $\overline{\alpha}$, $\overline{\beta}^{(0)}$ and $\overline{\beta}^{(2)}$ is given in Domke & Hubeny (1988) and Faurobert-Scholl (1991). In Table 9 we have given the values of the constants C_1, C_2, C_3 and C_4 which satisfy the normalization $\sum_{i=1}^{4}C_i=1$. Since Γ_I is orders of magnitude smaller than other rates, the models can be roughly characterized as elastic collision [Γ_C and $D^{(2)}$] dominated, except for model 5 for which the

Table 8. The effect of variation of the Planck function index m: $T^C=10^2$, $T_{opt}=21.5$, $T_{eff}=10^2$, $x_\epsilon=10^2$, $\tau_\epsilon=10^8$, $x_{\beta^C}=3.2$, $\tau_{\beta^C}=3.2\times10^3$, $x_{CS}=5.6$, $q=0.1$, $\langle N\rangle\simeq3.2\times10^3$, $\langle P\rangle\sim3.2\times10^{-4}$, $\langle l\rangle\sim10^4$, $x_{PD}=x_{FT}$, $\tau_{PD}=\tau_{FT}$, $B_m(r)=B_0r^m$, $s_R=[dB(r)/dr]_R=B_0mR^{m-1}$, $B_0=1$.

Model	m	s_R
1	−3	−0.037
2	−2	−0.074
3	−1	−0.111
4	+0	+0.000
5	+1	+1.000
6	+2	+6.000
7	+3	+27.000

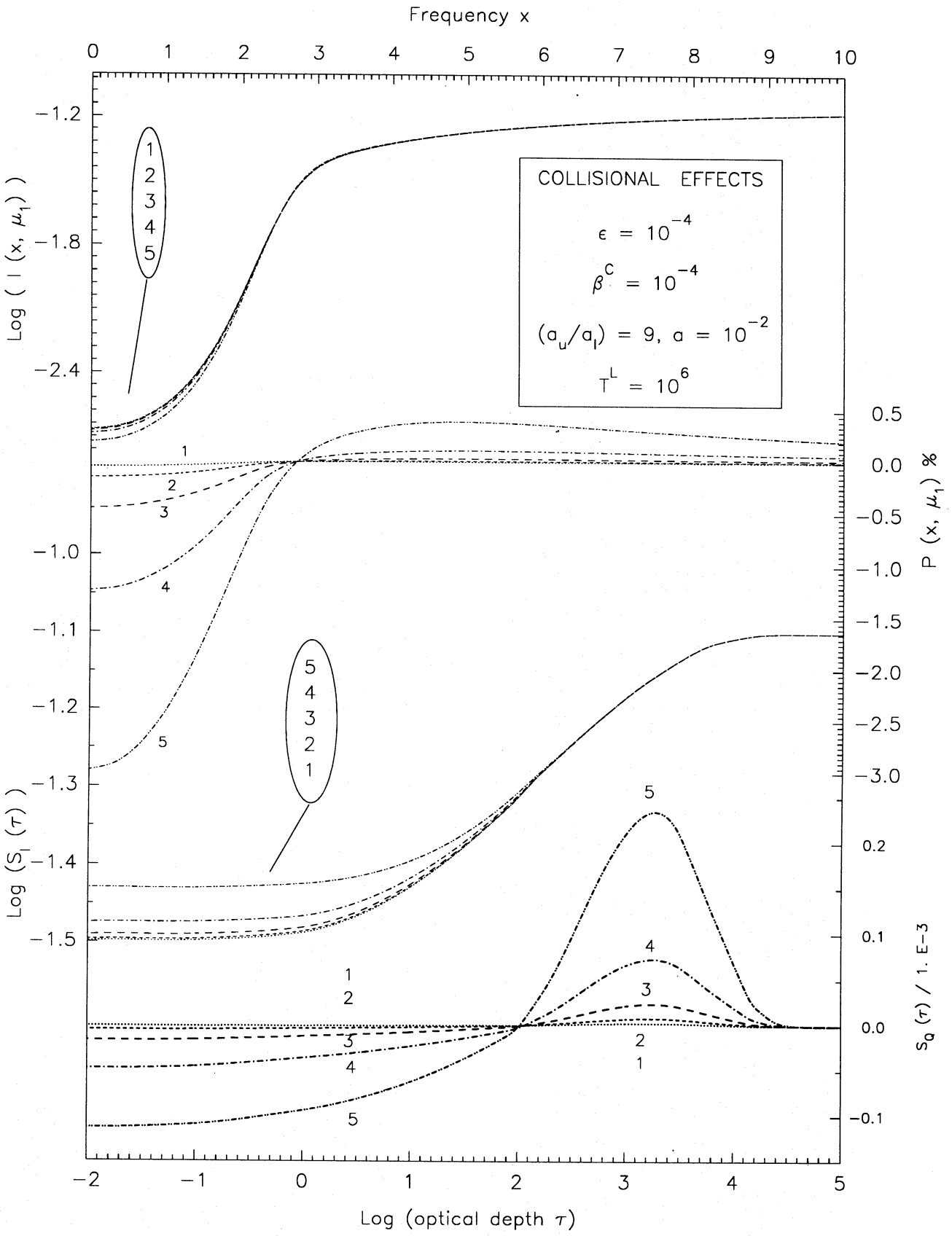

Figure 9. The effect of collisions on resonance line polarization. The exact Domke–Hubeny redistribution matrix is employed for the computations. See Section 2.9 and Table 9 for a discussion.

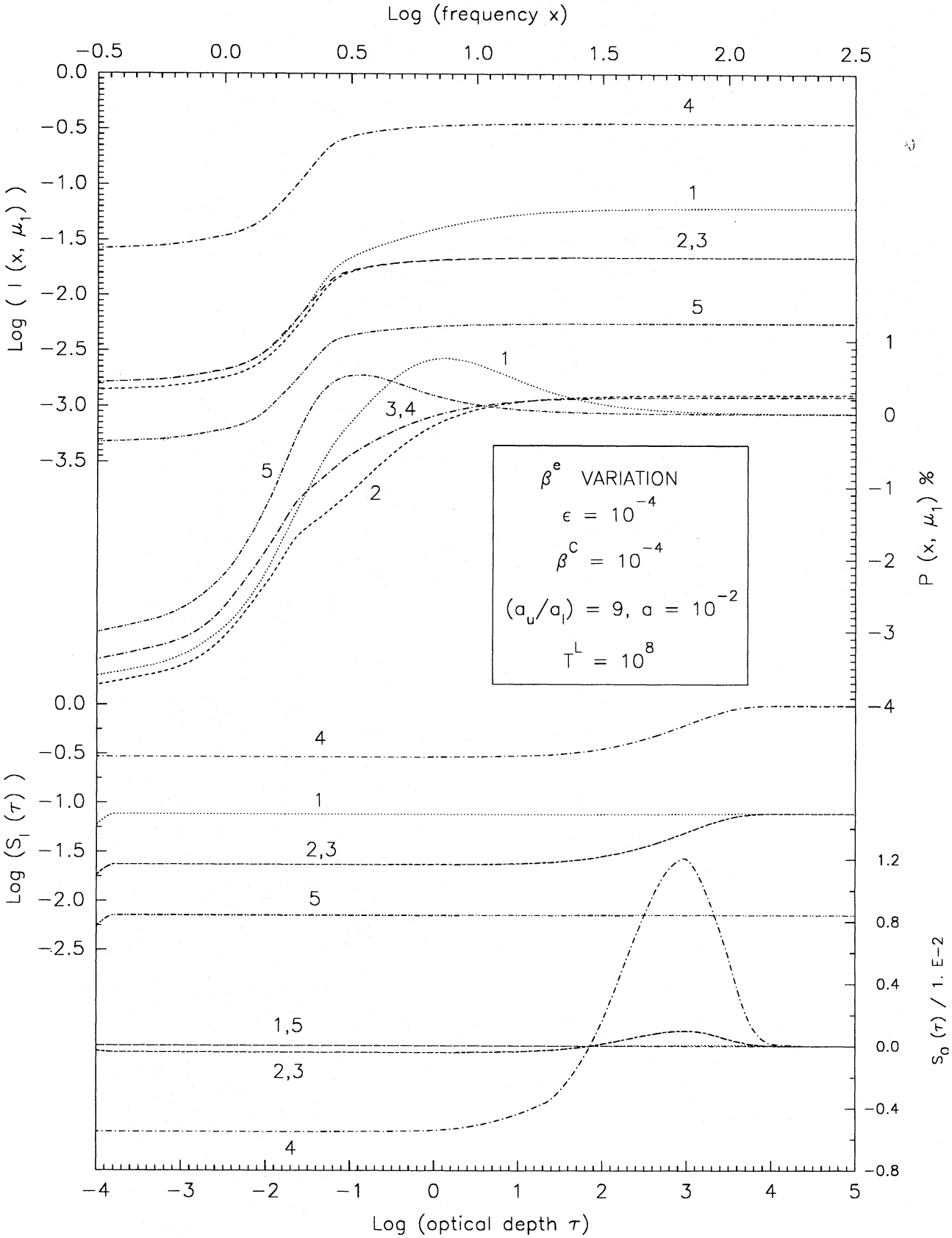

Figure 10. The effect of the electron scattering parameter $\beta^e = k^e/k^L$ on resonance line polarization (cf. Fig. 9). See Section 2.10 and Table 10 for further details. Note that frequency is expressed on a logarithmic scale.

radiative rate is as strong as the elastic collision rate. For this reason, the line polarization is already very small throughout the profile. The intensity profiles do not show any significant changes seen in polarization profiles. The strong changes seen in polarization profiles when going from model 1 to model 5 are basically due to large changes in the value of Γ_R by two orders of magnitude, and these cause a strong variation in the anisotropic part of scattering in the R_{II-A} redistribution matrix. For model 1, the polarization is extremely small throughout the profile. As with other sets of models in this paper, the crossover point from negative to positive polarization occurs for $x \leq x_{FT}$ and the maxima of polarized source functions $S_Q(\tau)$ occur around $\tau \leq \tau_{FT}$. It is important to note that the use of the DH collisional redistribution matrix provides a more exact treatment of partial redistribution effects in collision-dominated plasmas, and is as easy to use as the earlier version employing a branching ratio Λ between redistribution functions. The latter procedure is a special case of the former.

2.10 The effect of electron scattering on polarization of resonance lines scattering according to the Domke–Hubeny redistribution matrix

In this section, we show the effect of free-electron scattering on the wings of resonance lines (see Fig. 10 and Table 10). We select the value of $\beta^e = k^e(r)/k^L(r)$, where $k^e(r) = N_e \sigma_e$ is 10^{-3} when including electron scattering, which implies a significant electron density N_e in the atmosphere. The quantity σ_e is the classical Thomson scattering cross-section for free electrons. The electron scattering optical depth $T^e = \beta^e T^L = 10^5$ is sufficiently large to affect the polarization in the intermediate and far wings. Other model parameters employed in this section are: $\epsilon = 10^{-4}$; $\beta^C = 10^{-4}$; $a_u = 2.7 \times 10^{-2}$; $a_l = 0.3 \times 10^{-2}$; $a = a_u + a_l = 3 \times 10^{-2}$; $B(r) = 1$; $k^{L,C,e}(r) = Kr^{-2}$; $T^L = 10^8$ and $R = 3$. The collision broadening rates employed in the DH redistribution matrix are given in Table 10. Electron scattering is ignored in model 1. The model 2 represents coherent electron scattering (CES) in the atmosphere. The complete redistribution in electron scattering (model 3) is shown to be a good approximation by Mihalas, Kunasz & Hummer (1976). The electron scattering in general causes depression of the wing intensities of absorption profiles. While CES increases the core polarization, as well as the far-wing polarization, complete redistribution electron scattering (CRDE) decreases the polarization in the core and the near wings due to coupling with other parts of the profile. The polarization in the far wings ($x > 40$) remains nearly constant up to a large bandwidth and slowly goes over to zero, unlike the case of $\beta^e = 0$ when the polarization approaches zero for $x > 40$. Model 4 is identical to model 3 except for the geometry. It is interesting to note that although PP and SS intensities obviously differ by a large amount, the polarizations which depend purely on the number of anisotropic scatterings in the line-forming layers remain the same (for the $R = 3$ case). Model 5 shows the large differences in polarization and intensity profiles

Table 9. The effect of collisional redistribution on the resonance line: $a = 10^{-2}$, $\Delta\nu_D = 2.9 \times 10^9$ Hz, $\lambda_0 = 5000$ Å, $T_e = 5000$ K, $M^a = 40$ amu, $W_2 = 0.9$, $x_{PD} = x_{FT}$, $\tau_{PD} = \tau_{FT}$, $x_{FT} = 3.2$, $\tau_{FT} = 3.2 \times 10^3$.

Model	f	Γ_C	Γ_R	$D^{(2)}$	Γ_I	C_1	C_2	C_3	C_4
		Hz	Hz	Hz	Hz				
1	$0.86\ 10^{-3}$	$0.36\ 10^{9}$	$0.25\ 10^{7}$	$0.14\ 10^{9}$	$0.25\ 10^{3}$	0.006	0.001	0.010	0.983
2	$0.26\ 10^{-2}$	$0.35\ 10^{9}$	$0.74\ 10^{7}$	$0.13\ 10^{9}$	$0.74\ 10^{3}$	0.018	0.002	0.029	0.951
3	$0.77\ 10^{-2}$	$0.34\ 10^{9}$	$0.22\ 10^{8}$	$0.12\ 10^{9}$	$0.22\ 10^{4}$	0.056	0.006	0.077	0.861
4	$0.23\ 10^{-1}$	$0.29\ 10^{9}$	$0.67\ 10^{8}$	$0.11\ 10^{9}$	$0.67\ 10^{4}$	0.166	0.019	0.170	0.645
5	$0.70\ 10^{-1}$	$0.16\ 10^{9}$	$0.20\ 10^{9}$	$0.61\ 10^{8}$	$0.20\ 10^{5}$	0.498	0.056	0.191	0.255

Table 10. The effect of electron scattering on line polarization: $a = 3 \times 10^{-2}$, $\Delta\nu_D = 2.9 \times 10^9$, $W_2 = 0.9$, $\Gamma_R = 8.8 \times 10^8$, $\Gamma_C = 2 \times 10^8$, $\Gamma_I = 8.9 \times 10^5$, $D^{(2)} = 0.758 \times 10^8$, $\beta = \beta^C + \beta^e$, $T_{eff} = 10^4$, $T^C = \beta T^L = (10^4, 11 \times 10^4)$, $T_{opt} = 144$, $x_{PD} = x_{FT}$, $\tau_{PD} = \tau_{FT}$.

Model	$R^e_A(x,x')$	β^e	R	β	x_{FT}	τ_{FT}	x_{CS}	$<N>$	$<P>$	$<I>$	q
		$\times 10^{-3}$		$\times 10^{-3}$							
1	0	0	3	0.1	4.2	$2.4\ 10^3$	9.8	$2.4\ 10^3$	$4.2\ 10^{-4}$	10^4	0.033
2	CES	1	3	1.1	2.3	$4\ 10^2$	3.0	$4\ 10^2$	$2.5\ 10^{-3}$	$9.1\ 10^3$	0.36
3	CRES	1	3	1.1	2.3	$4\ 10^2$	3.0	$4\ 10^2$	$2.5\ 10^{-3}$	$9.1\ 10^3$	0.36
4	CRES	1	1	1.1	2.3	$4\ 10^2$	3.0	$4\ 10^2$	$2.5\ 10^{-3}$	$9.1\ 10^3$	0.36
5	0	1	3	1.1	2.3	$4\ 10^2$	3.0	$4\ 10^2$	$2.5\ 10^{-3}$	$9.1\ 10^3$	0.36

when electron scattering opacity is treated as true continuum absorption and added on to β^C, instead of being treated as a scattering process. Notice that x_{CS} correspond to the maxima of polarization curves and x_{FT} give their crossover frequencies when electron scattering is not treated as redistribution (models 1 and 5). However, the introduction of electron redistribution (models 2, 3 and 4) produces polarization curves for which the asymptotic expressions are no longer useful due to predominance of electron redistribution over atomic redistribution in the intermediate and far-wing frequency points.

3 CONCLUSIONS

In this paper, we have shown the effect of collisions on line polarization through a large number of schematic models. For the set of 'standard model' parameters employed, there are no significant differences between the frequency dependence of linear polarization profiles of resonance and subordinate lines, even including collisions. It is important to note that the 'standard model' employed here, in most of the computations, represents a rather weak line, formed under a strong background continuum opacity. Observed typical stellar photospheric lines, however, are characterized by much smaller values of ϵ and β^C, and the branching ratio $\Lambda \rightarrow 1$. Such a choice of .odel parameters for strong lines indeed brings out the intrinsic physical difference between resonance and subordinate line partial redistribution mechanisms more clearly, as demonstrated by Hubeny & Heinzel (1984). Thus the lack of a significant difference between the results for resonance line and subordinate line redistribution in this paper is mainly due to the somewhat larger values of both ϵ and β, and a smaller value of coherence fraction Λ employed by us. So our 'standard model' does not necessarily represent typical stellar atmospheric conditions. I am grateful to the referee for having pointed out this fact, which places the results discussed in this paper into a proper context. Variation of macroscopic parameters such as radial extent (R) of the spherical shell, and the index (m) of the power-law dependence of the Planck function on radius (r) have individual characteristic effects on the emergent intensity and polarization. It is not always true that line polarization changes are more sensitive than scalar specific intensity changes to variation of physical and geometrical parameters, as demonstrated through the variation of the opacity and the Planck function with radius. Indeed, the polarization changes are stronger only if the number of angularly anisotropic scatterings are affected by radiative transfer in the relevant layers where the line is formed. The geometric parameter that can dramatically change the frequency dependence of polarization profile is the outer radius (R) of a spherical atmosphere, basically through the strong changes in the limb darkening caused by this parameter. It is clear that proper care is necessary when modelling the linear polarization profiles in spherical shells with large radial extent. An exact treatment of collisions in polarized PRD computations is now possible with the use of the Domke–Hubeny polarized redistribution matrix. It can quantitatively incorporate specific kinds (phase- and alignment-changing elastic collisions, inelastic collisions, etc.) of the collisional line broadening into the transfer problem without difficulty. However, for a preliminary analysis, the simpler approach of using linear combinations of PRD redistribution functions is sufficient. The electron redistribution mechanism affects the line wings, in the presence of collisional redistribution, basically through its ability to induce large frequency shifts on each scattering. For both the resonance and subordinate lines formed in spherically symmetric model atmospheres, the escape probability expressions of planar media can be employed to a reasonable approximation.

ACKNOWLEDGMENTS

I am grateful to the referee for very useful comments and suggestions. I also thank Dr Helene Frisch for a helpful discussion about the scaling laws in line transfer theory.

REFERENCES

Domke H., Hubeny I., 1988, ApJ, 334, 527
Faurobert-Scholl M., 1987, A&A, 178, 269
Faurobert-Scholl M., 1988, A&A, 194, 268
Faurobert-Scholl M., 1991, A&A, 246, 469
Faurobert-Scholl M., 1992, A&A, 258, 521
Faurobert-Scholl M., 1993, A&A, 268, 765
Frisch H., 1980, A&A, 83, 166
Frisch H., 1984, in Kalkofen W., ed., Methods in Radiative Transfer. Cambridge Univ. Press, Cambridge, p. 65
Frisch H., 1988, in Kudritzki R. P., Yorke H. W., Frisch H., eds, Radiation in Moving Gaseous Media. SAAS-FEE, Geneva Observatory, Switzerland, p. 337
Heinzel P., Hubeny I., 1982, J. Quant. Spectros. Radiat. Transfer, 27, 1
Hubeny I., 1985a, A&A, 145, 463
Hubeny I., 1985b, in Beckman J. E., Crivellari L., eds, NATO ASI Ser. C, 152. Progress in Stellar Spectral Line Formation Theory. Reidel, Dordrecht, p. 27
Hubeny I., Heinzel, P., 1984, J. Quant. Spectros. Radiat. Transfer, 32, 159
Hummer D. G., Kunasz P. B., 1980, ApJ, 236, 609
Ivanov V. V., 1970, Astrophysics, 6, 355
Ivanov V. V., 1991, In Crivellari L., Hubeny I., Hummer D. G., eds, NATO ASI Ser. C, 341, Stellar Atmospheres: Beyond Classical Models. Kluwer, Dordrecht, p. 81
Kunasz P. B., Hummer D. G., 1974, MNRAS, 166, 19
Mihalas D., Kunasz P. B., Hummer D. G., 1976, ApJ, 210, 419
Nagendra K. N., 1986, PhD thesis, Bangalore Univ.
Nagendra K. N., 1988, ApJ, 335, 269
Nagendra K. N., 1989, Ap&SS, 154, 119
Nagendra K. N., 1994, ApJ, 432, 274
Omont A., Smith E. W., Cooper J., 1972, ApJ, 175, 185
Rees D. E., 1987, in Kalkofen W., ed., Numerical Radiative Transfer. Cambridge Univ. Press, Cambridge, p. 213
Rees D. E., Murphy G. A., 1987, in Kalkofen W., ed., Numerical Radiative Transfer. Cambridge Univ. Press, Cambridge, p. 241
Rees D. E., Saliba G. J., 1982, A&A, 115, 1
Saliba G. J., 1985, Sol. Phys., 98, 1